JOURNAL OF MATERIALS SCIENCE 19 (1984) 2387–2395

Mechanical models to describe the behaviour of polyaramid fibres

J. R. WHITE *
Polymer Science and Engineering, University of Massachusetts, Amherst, Mass. 01003, USA

T. J. LARDNER
Civil Engineering Department, University of Massachusetts, Amherst, Mass. 01003, USA

Mechanical models which imitate the behaviour of polyaramid fibres are discussed. The models were developed from a phenomenological standpoint but the parameters which characterize certain of the elements in the model agree fairly closely with measured elastic properties, suggesting that structural analogies may exist between the model and the material.

1. Introduction

Mechanical models are frequently employed to imitate the deformation behaviour of solid polymers. They are of value (a) if they help to indicate a convenient mathematical representation of the behaviour of the real material, permitting interpolation and sometimes (but with caution) extrapolation; (b) if they predict critical or limiting conditions; and (c) if they indicate the kind of molecular mechanism that may be responsible for the observed deformation. Spring and dashpot models are common in the polymer literature, most often in the form of the Maxwell body (spring and dashpot in series), the Voigt–Kelvin body (spring and dashpot in parallel), or the standard linear solid, which has three elements (two springs plus one dashpot, or one spring and two dashpots). The most popular form of the standard linear solid has a spring in parallel with a Maxwell body, and has been shown to have a constitutive equation identical to the one derived using the two-site model theory of thermally activated deformation and simplified using certain approximations [1].

The purpose of this paper is to develop a model which predicts compressive buckling in a rigid-rod polymer fibre, and which also predicts the form of the stress–strain characteristic under tensile loading subsequent to buckling.

2. The Model

The basic model is shown in Fig. 1. This is adequate to account for the buckling instability, but has to be modified to reproduce the observed tensile behaviour of buckled fibres.

A conventional spring-and-dashpot model with all elements parallel does not lead to the prediction of buckling under compressive loads. A simple method of providing an element which buckles under a vertical load is shown in Fig. 1. AB and BC are rigid rods, connected together at B. The point A is fixed, but AB may rotate about A within the plane of the diagram. BC is connected at C to a spring (denoted S_1) of stiffness E_1. The connections at B and C also permit free rotation within the plane of the diagram, but do not allow movement normal to the plane. C is constrained to remain vertically below A.

2.1. Behaviour in uniaxial compression

When a vertical compressive force is directed along XA the assembly will tend to buckle. This deformation will be opposed by a restoring force provided along DB by the horizontal spring

* Permanent address: Department of Metallurgy and Engineering Materials, University of Newcastle upon Tyne, Newcastle upon Tyne NE1 7RU, UK

0022–2461/84 $03.00 + .12

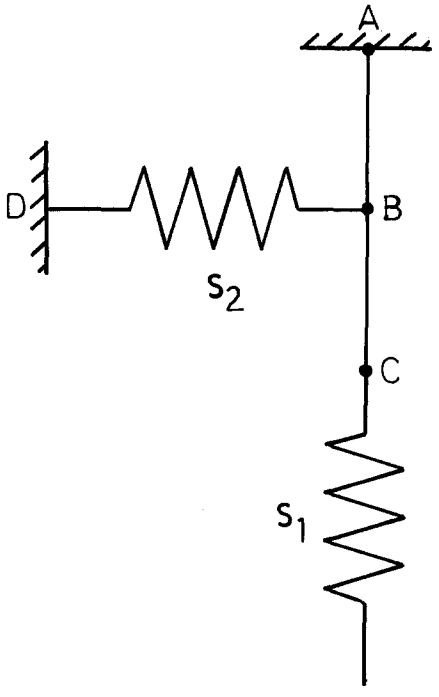

Figure 1 Basic model consisting of two springs, S_1 and S_2, and two rigid rods, AB and BC. Points A and D are fixed. AB and BC may rotate in the plane of the diagram and C is constrained to remain vertically below A.

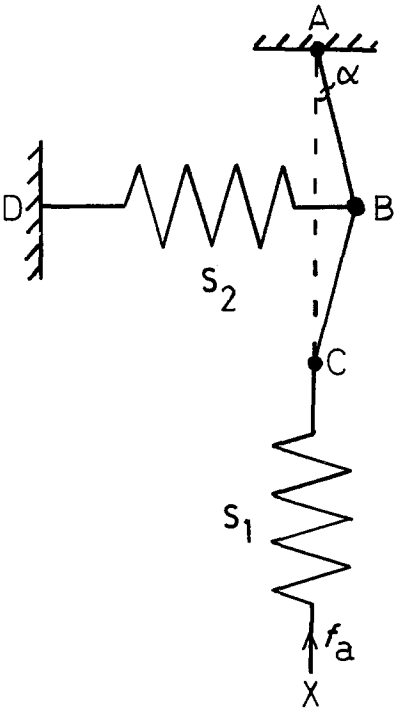

Figure 2 Deformation of the model under a vertical compressive load, F_a. Buckling of the rigid-rod assembly ABC is shown by displacement, α, to the vertical. This will not occur until a critical force is applied.

(denoted S_2), of stiffness E_2, which will prevent buckling until a limiting condition is reached. This limiting condition can be derived by reference to Fig. 2, in which a small angular displacement, α, has been given to the rigid rods. If AB, BC and the two springs all have unit length, and if the applied vertical force is f_a, then the force along CB and along BA is $f_a/\cos\alpha$ and the force along BD is therefore $2f_a \sin\alpha/\cos\alpha$. The strain in S_2 is $\sin\alpha$ so that the restoring force is $E_2 \sin\alpha$. Hence, if $E_2 \sin\alpha > 2f_a \sin\alpha/\cos\alpha$ then buckling will not occur. That is, buckling will not occur as long as

$$f_a < \frac{E_2}{2}\cos\alpha \qquad (1a)$$

or

$$f_a < E_2/2 \qquad (1b)$$

(α assumed small).

In the above analysis it has been assumed that the horizontal spring is linear with stiffness E_2. With such an element the small-strain tensile behaviour of the assembly will not imitate the measured characteristics [2], and to overcome this problem the linear spring may be replaced with one which has the following nonlinear behaviour:

$$F_2 = E_2\epsilon_2 = K_2 \sin\frac{\pi\epsilon_2}{\epsilon_{2,m}} = K_2 \sin\frac{\pi \sin\alpha}{\epsilon_{2,m}}$$

where F_2 is the force along BD, ϵ_2 is the strain in the horizontal spring (= $\sin\alpha$), $\epsilon_{2,m}$ is the maximum strain of spring S_2 and K_2 is a constant. (In this version of the model, E_2 is not a constant.)

The instability condition can be defined in the same way as before and if the perturbation, α, is considered to be sufficiently small that $\sin\alpha \ll \epsilon_{2,m}$, so that the small-angle approximation can be made for $\sin[(\pi \sin\alpha)/\epsilon_{2,m}]$, then

$$E_2 \to \frac{K_2\pi}{\epsilon_{2,m}}$$

This leads to an equivalent condition to that given in (Equation 1b), i.e.

$$f_a < \frac{K_2\pi}{2\epsilon_{2,m}} = f_c$$

Once this critical value of f_a is exceeded then buckling occurs and if loading is performed under deformation-controlled conditions then the

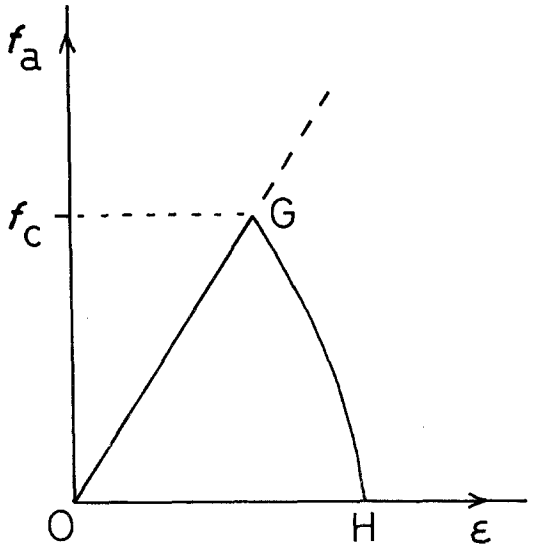

Figure 3 Force–strain diagram in compression for the body shown in Fig. 2 where S_2 is a nonlinear spring. G is the point at which buckling occurs and H represents the unloaded state corresponding to $\epsilon_2 = \epsilon_{2,m}$ in the element F_2.

element spontaneously moves to the first unloaded state at which $\epsilon_2 = \epsilon_{2,m}$ (see Fig. 3). At this point the angle of AB and of BC to the vertical has the limiting value $\alpha = \alpha_0$ given by $\epsilon_{2,m} = \sin \alpha_0$.

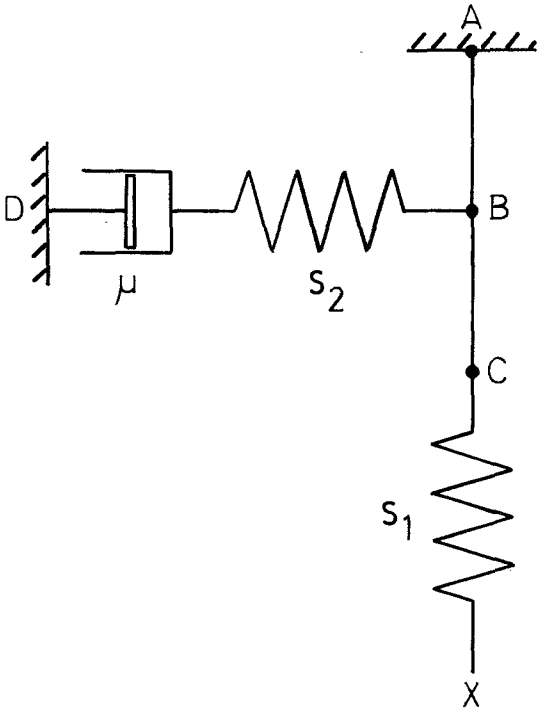

Figure 4 Model modified by the addition of a dashpot, stiffness μ, in the horizontal member BD.

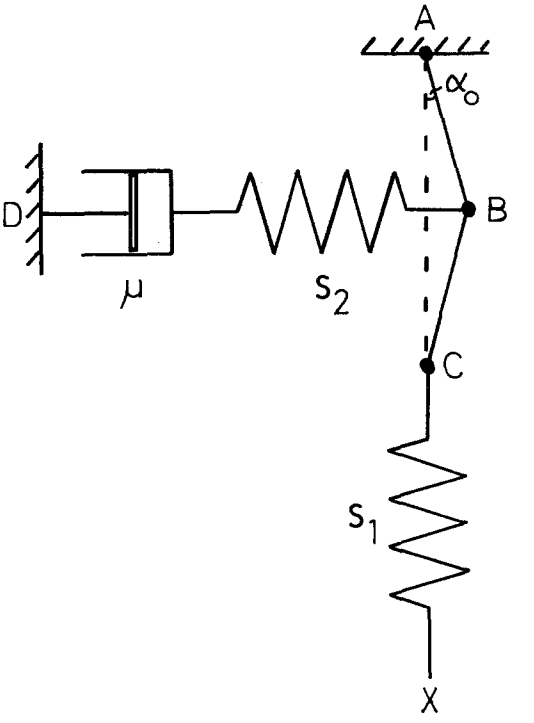

Figure 5 Buckled model just before applying a vertical tensile force, f_b, showing the setting angle, α_0.

The purpose of this modification, i.e. the introduction of a nonlinear spring, is to model the behaviour of a buckled fibre under subsequent tension, but before the analysis of tensile loading let us consider an alternative mechanical model that might also be used to account for buckling and the subsequent tensile characteristics. This is shown in Fig. 4, in which the horizontal spring has been replaced by a linear spring, stiffness E_2, and dashpot, stiffness μ.

If we choose to have a very stiff dashpot (μ large) then it can be assumed that negligible deformation takes place within the dashpot during the timescale of the initial compressive deformation, so that the buckling behaviour is exactly the same as that analysed above for the model shown in Fig. 1. Let us now assume that once buckling has been completed the body is allowed to rest for sufficient time for the dashpot to relax the spring S_2; thereafter the external load is removed. The body will now take up the configuration shown in Fig. 5, with no stress along BD. AB and BC are tilted at α_0 to the vertical (kinked or buckled condition).

However, whereas this model using a linear spring and a linear dashpot is attractive since it uses elements common in the modelling of solid

polymer behaviour, it suffers from the defect that in the presence of an initial imperfection (i.e. a nonzero tilt, α) any applied compressive load however small will cause the model to buckle in time. The presence of the nonlinear spring in the earlier model allows "elastic behaviour" with buckling from the straight configuration to the configuration defined by $\epsilon_{2,m}$.

2.2. Behaviour in uniaxial tension

If a vertical tensile force f_b is applied to the (undeformed) body shown in Fig. 1 then the spring with stiffness E_1 takes up the total deformation and the constitutive equation can be written

$$f_b = \epsilon_1 E_1$$

where ϵ_1 is the strain in spring S_1. Since the strain in the rigid-rod assembly, ABC, is zero, the net strain in AX is $\epsilon_1/3$ $(= \epsilon)$, so that:

$$f_b = 3\epsilon_1 E_1.$$

Now let us consider a similar test conducted on a body which has previously buckled in compression.

2.2.1. Nonlinear spring model

Consider Fig. 2. In the buckled state under no external loading AB and BC will be at the limiting angle $\alpha = \alpha_0$ to the vertical. When a tensile force, f_b, is directed along AX the spring S_1 will deform and in addition the assembly ABC will tend to align itself to the vertical. The restoration of ABC to the straight (vertical) configuration will be resisted by the horizontal element, S_2. The deformation in S_1 is $\epsilon_1 = f_b/E_1$. The deformation in the rigid-rod assembly can be obtained by considering the equilibrium conditions at C and B. In CB the force is $f_b/\cos\alpha$ and the force along BD will therefore be $2f_b \sin\alpha/\cos\alpha$. Hence, the deformation of S_2 (nonlinear) will be given by:

$$2f_b \frac{\sin\alpha}{\cos\alpha} = K_2 \sin\frac{\pi \sin\alpha}{\sin\alpha_0}$$

or

$$\frac{2f_b\epsilon_2}{\cos\alpha} = K_2 \sin\frac{\pi\epsilon_2}{\epsilon_{2,m}}$$

i.e.

$$f_b = \frac{K_2}{2\epsilon_2}(1-\epsilon_2^2)^{1/2} \sin\frac{\pi\epsilon_2}{\epsilon_{2,m}} \qquad (2)$$

For the case of small angles,

$$f_b = \frac{K_2}{2\alpha}\sin\frac{\pi\alpha}{\alpha_0} \qquad (2a)$$

We note that as α varies from α_0 to zero, the value of f_b varies from zero to the previously determined buckling load (i.e. $K_2\ \pi/2\alpha_0$). That is, the value of the tensile load required to straighten the structure ABC is equal to the critical buckling load. Now, the contribution to deformation by the rigid-rod assembly is $2(\cos\alpha - \cos\alpha_0) = (\alpha_0^2 - \alpha^2) \equiv (\epsilon_{2,m}^2 - \epsilon_2^2)$. Hence, the total strain (appropriately weighted to account for the lengths of the component elements) is

$$\epsilon = \frac{f_b}{2E_1} + \frac{1}{3}(\alpha_0^2 - \alpha^2) = \frac{f_b}{3E_1} + \frac{1}{3}(\epsilon_{2,m}^2 - \epsilon_2^2) \qquad (3)$$

where $\epsilon_2(f_b)$ is given by Equation 2.

By appropriate choice of fitting parameters in Equations 2 and 3, the tensile behaviour shown by compressed fibres [2] can be reproduced approximately.

At this stage it is convenient to introduce an approximation that leads to a form of the expression for the strain, $\epsilon(f_b)$, which will provide a useful comparison with a result derived in a later section. The approximation we introduce here is as follows:

$$f_b = \frac{K_2}{2\alpha}\sin\frac{\pi\alpha}{\alpha_0} \simeq \frac{K_2\pi}{2\alpha_0}\left(1 - \frac{\alpha}{\alpha_0}\right) \qquad (2b)$$

Essentially, this approximation can be written $\sin x \simeq x(1 - x/\pi)$. The function $\sin x/x\ (1 - x/\pi)$ shows a monotonic increase from unity (at $x = 0$) to a maximum of $4/\pi$ at $x = \pi/2$, indicating that the proposed substitution does not seriously alter the analysis. It then follows that $\alpha \simeq \alpha_0\ (1 - f_b/f_c)$, where $f_c = K_2\pi/2\alpha_0$, and using this approximate expression for α we can rewrite the total-strain expression in the approximate form

$$\epsilon = \frac{f_b}{3E_1} + \frac{\alpha_0^2}{3}[1 - (1 - f_b/f_c)^2] \qquad 0 \leqslant f_b \leqslant f_c \qquad (4a)$$

Once the load in tension equals f_c the rods are straight and the total-strain expression becomes

$$\epsilon = \frac{f_b}{3E_1} + \frac{\alpha_0^2}{3} \qquad f_c \leqslant f_b \qquad (4b)$$

Subsequent loading then corresponds to the

response of the linear spring, S_1. By appropriate choice of fitting parameters in Equations 4a and 4b the tensile behaviour shown by compressed fibres can be reproduced approximately.

2.2.2. Model in which restoring force is provided by a Maxwell body

In the previous section we showed how the non-linear model provides a description of the tensile behaviour of previously compressed fibres. In this section, we discuss the case of a Maxwell body and note, as in the case of the prediction of the buckling load, that whereas this model can provide an approximate expression for the total strain it suffers some defects. Consider the configuration shown in Fig. 5, and let us assume that the tensile test is conducted in a time sufficiently short for the motion of the dashpot to be negligible.

On applying a vertical tensile force, f_b, along AX the spring S_1 and the rigid-rod assembly will both deform, as described in the previous section. As before, the total strain, ϵ, is given by Equation 3 where $\epsilon_{2,m} \equiv \sin \alpha_0$ and $\epsilon_2 = \sin \alpha$ and where α is the angle of AB and BC to the vertical when f_b is the applied force and α_0 is the buckled value of α before application of the tensile force. It is convenient to make the small-angle approximation so that Equation 3 can be written:

$$\epsilon = \frac{f_b}{3E_1} + \tfrac{1}{3}(\alpha_0^2 - \alpha^2) \tag{3a}$$

The strain in the horizontal element is

$$\sin \alpha_0 - \sin \alpha = \alpha_0 - \alpha$$

(referred to the buckled starting configuration). From a consideration of force equilibrium at B we can write

$$2f_b \sin \alpha / \cos \alpha = E_2(\alpha_0 - \alpha) = 2f_b\alpha(1 + \alpha^2/2) \tag{5a}$$

Or, if α is small,

$$2f_b\alpha = E_2(\alpha_0 - \alpha) \tag{5b}$$

or

$$f_b = \frac{E_2}{2}\frac{\alpha_0 - \alpha}{\alpha}$$

In contrast to the case with the nonlinear spring, we note that f_b varies from zero when $\alpha = \alpha_0$ to infinitely large values when $\alpha = 0$. If, however, we solve for α and substitute into Equation 3a we find

$$\epsilon = \frac{f_b}{3E_1} + \frac{\alpha_0^2}{3} - \frac{E_2^2\alpha_0^2}{3(E_2 + 2f_b)^2} \tag{6}$$

In this expression f_b can range from zero to arbitrarily large values without consideration of separate expressions corresponding to straightening of the rigid rods, as in Equations 4a and 4b.

Equation 6 can be written in the form:

$$\epsilon = \frac{f_b}{3E_1} + \frac{\alpha_0^2}{3}\left[1 - \frac{1}{(1 + 2f_b/E_2)^2}\right] \tag{7}$$

This expression should be contrasted with Equations 4a and 4b.

It is instructive to differentiate this expression with respect to f_b in order to examine its properties, i.e.

$$\frac{d\epsilon}{df_b} = \frac{1}{3E_1} + \frac{4\alpha_0^2}{3E_1(1 + 2f_b/E_2)^3}$$

When f_b is large $d\epsilon/df_b \to 1/3E_1$, as for the body tested in tension without a preliminary compressive buckling. At small values of f_b the gradient $d\epsilon/df_b$ is larger (i.e. $df_b/d\epsilon$ is smaller), indicating a smaller initial modulus. The modulus is predicted to rise towards the limiting value of $3E_1$ as f_b gets larger.

3. Results

Fig. 6 shows the load-deformation behaviour obtained by DeTeresa [3] for a sample of Kevlar 49. Also shown is the form of Equation 7 when $3E_1 \equiv 145\ \mathrm{GN\,m^{-2}}$ (the measured tensile modulus of the as-prepared fibre and the limiting slope of the characteristic obtained with buckled fibres tested in tension), $\alpha_0^2/3 \equiv 0.0214$ and $E_2 \equiv 0.32\ \mathrm{GN\,m^{-2}}$. These parameters were obtained by curve fitting. The value of α_0 so derived is thus approximately 14.5°, and the small-angle approximation used to obtain Equation 7 is therefore not unreasonable. The value E_2 obtained here leads to the prediction that buckling may occur when the compressive stress exceeds $0.16\ \mathrm{GN\,m^{-2}}$. This is a rather low value, but there are few experimental data with which to compare it. DeTeresa *et al.* [2] indicate that buckling occurs for a compressive strain $< 3\%$, which gives an upper limit of $4.35\ \mathrm{GN\,m^{-2}}$ for the corresponding stress using their value of $145\ \mathrm{GN\,m^{-2}}$ for Young's modulus. More recent measurements [3] show that buckling occurs at strains much closer to 0.3%, giving much better agreement with the

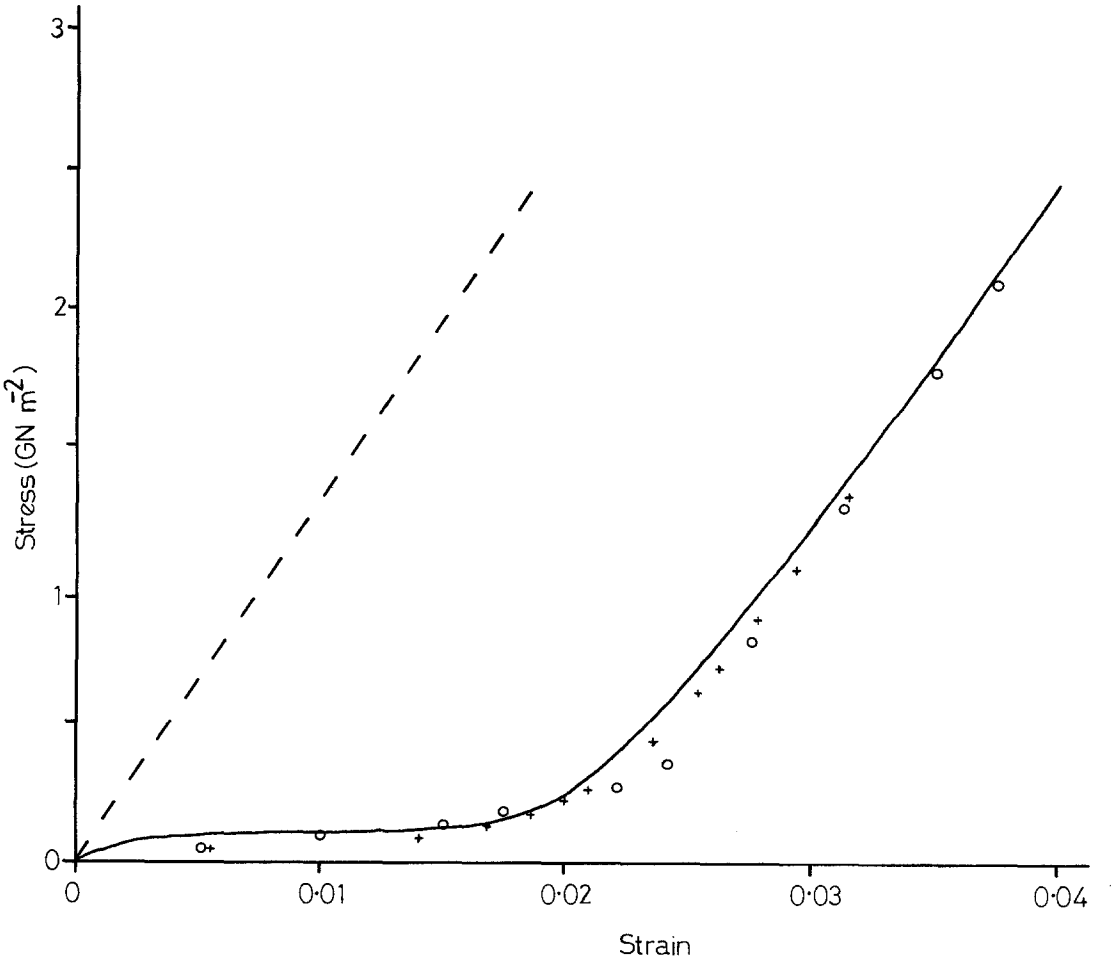

Figure 6 Stress–strain data obtained in tension by DeTeresa for (a) as received Kevlar 49 (broken line) and (b) Kevlar 49 which had been subjected to compression (solid line). The crosses show points satisfying Equation 7 when $f_b/3E_1 = 145\,\mathrm{GN\,m^{-2}}$, $\alpha_0^2/3 = 0.0214$ and $E_2 = 0.32\,\mathrm{GN\,m^{-2}}$. The open circles show points satisfying Equations 4a and 4b if $f_b/3E_1 = 145\,\mathrm{GN\,m^{-2}}$, $\alpha_0^2/3 = 0.0214$ and $f_c = 0.4\,\mathrm{GN\,m^{-2}}$.

model. It is also notable that the value of E_2 is reasonably close to the value of the transverse modulus of Kevlar 49 ($= 0.76\,\mathrm{GN\,m^{-2}}$), obtained by Phoenix and Skelton [4].

In the model corresponding to Equations 4a and 4b let us choose to take

$$\frac{\alpha_0^2}{3} = 0.0124$$

$$3E_1 = 145\,\mathrm{GN\,m^{-2}}$$

and

$$f_c = \frac{K_2\pi}{2\alpha_0} = 0.4\,\mathrm{GN\,m^{-2}}$$

A plot of values obtained from Equations 4a and 4b is also included in Fig. 6. It is clear from Fig. 6 that both models provide reasonable approximations to the behaviour of a compressed fibre in tension while at the same time providing a description of the kinking of fibres under compression.

4. Discussion

The model presented here reproduces the essential features of the behaviour of polyaramid fibres when tested parallel to the fibre axis. The limiting compressive strength has been derived from the model using data obtained in tension only on a previously buckled fibre. Mechanical models are notorious for the lack of agreement between the parameters required to fit behaviour under different modes of loading, so this result should not be taken too seriously without further investigation. It does indicate, nevertheless, the need to

increase the fibre stiffness perpendicular to the fibre axis in order to improve the capability of the fibres and their composites in compression.

The version of the model presented in Figs. 1 and 2 in which S_2 was given nonlinear (sinusoidal) behaviour does not lead to any simple molecular analogy because of the unusual form of the deformation of this horizontal element. The Maxwell body which replaces it in Figs. 4 and 5 is much more familiar, and can be taken to model a combination of elastic deformation (bond stretching, bond-angle deformation), and viscous flow or conformational changes, as in many conventional simple analyses of viscoelasticity. It is for this reason, as well as because this version of the model gives a more convenient mathematical form, that we suggest that it can be used effectively as long as its limitations are understood.

The model includes what appears to be an innovation in polymer mechanics, namely the introduction of rigid rods. It is necessary to consider whether this innovation is essential and/or useful or instructive. It is interesting to consider whether it has any structural significance, but before dwelling on these matters we will anticipate a result obtained below where the model is further modified to eliminate the rigid rods. Hence, we will here simply observe that the structural analogue to the model shown in Figs. 4 and 5 would probably consist of hard and soft segments in series, with the soft segments having stiffness E_1 and the hard segments a much higher stiffness, giving negligible deformation in the axial (vertical) direction. If the hard segments were hinged so that in compression they tended to collapse in the same manner as the model before the soft segments failed, it is possible that a quite close analogy might be established. Whereas such materials may exist and may be of importance, they are not the subject under scrutiny here, and the model may be further modified to eliminate the rigid rods.

Although the idea of modelling "rigid rod molecule" behaviour with rigid-rod elements might appear to be appealing, the latter are assumed to be infinitely stiff and can therefore be of limited value only in imitating real materials. Thus we have examined the properties of the body shown in Fig. 7 in which the rigid rods AB, BC have been replaced by stiff springs of equal stiffness, E_a. The presence of these deformable elements removes the need for the element shown in Figs. 1, 2, 4 and 5 as S_1. The springs AB and BC now shorten under compressive loading, but the instability is still governed by the restoring force along BD and it is easily seen that the same instability condition ($f_a \geqslant E_2/2$) exists.

To derive the behaviour of the body in tension after compressive buckling the same procedure is used as before, with the springs AB and BC beginning with a setting angle α_0 to the vertical, as shown in Fig. 8. Again, the body is assumed to reside for sufficient time in the unloaded condition to release the springs through the operation

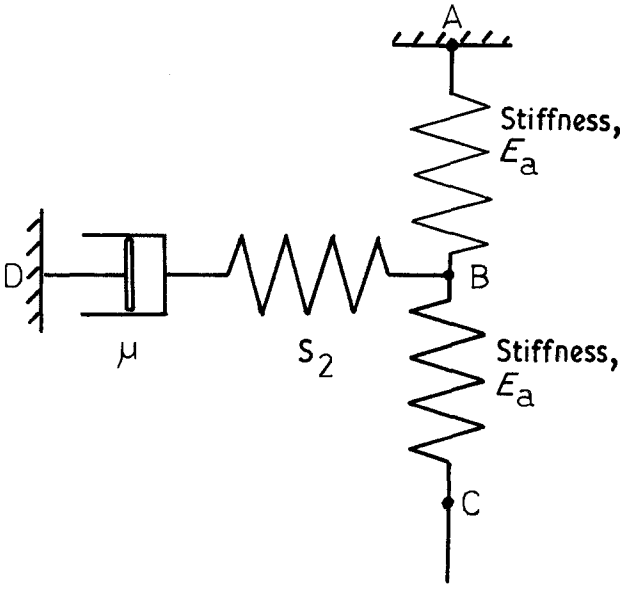

Figure 7 Model in which rigid rods have been eliminated. The two springs AB and BC have the same stiffness, E_a. The points A, B, C and D have the same constraints as in Fig. 1.

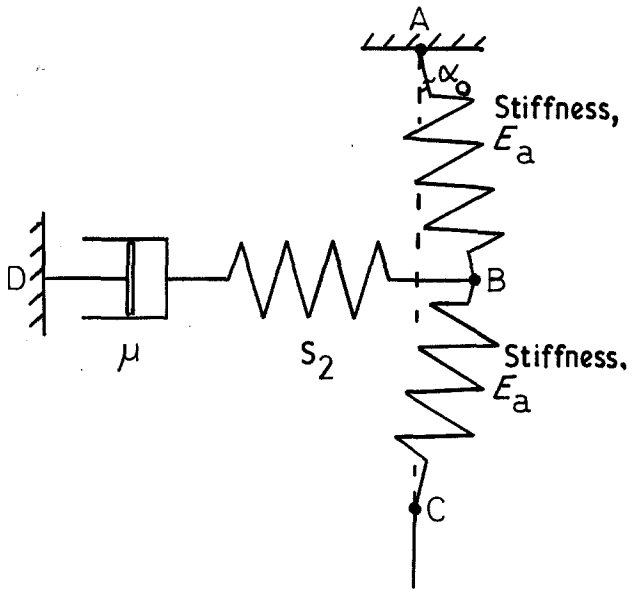

Figure 8 The model shown in Fig. 7 after buckling in compression to a setting angle, α_0.

of viscous processes before commencing with the tensile test. Now the strain in AB and BC must be taken into account as well as the contribution that comes from reducing α_0 to a smaller value α when under a tensile load f_b. Hence, the strain now becomes

$$\epsilon = \frac{f_b}{E_a} + (\cos\alpha - \cos\alpha_0) = \frac{f_b}{E_a} + \frac{1}{2}(\alpha_0^2 - \alpha^2) \tag{8}$$

In the horizontal element we have, as before (Equation 5b),

$$E_2(\alpha_0 - \alpha) = 2f_b\alpha$$

and on substituting for α in Equation 8 the expression for the strain becomes:

$$\epsilon = \frac{f_b}{E_a} + \frac{\alpha_0^2}{2}\left[1 - \frac{1}{(1 + 2f_b/E_2)^2}\right] \tag{9}$$

This is identical in form to Equation 7, and its use would have lead to the same value of E_2 as found above. α_0 would now become 12° ($\alpha_0^2/2 = 0.0214$). Therefore, it is not necessary to invoke the use of rigid-rod elements.

Thus, on reference to Figs 7 and 8, we may now speculate that an analogy exists between our mechanical model and a so-called rigid-rod molecule or rigid-rod molecule fibril. The high axial stiffness is modelled by stiff springs which are hinged, leading to the possibility of buckling under compressive loads. The hinges could be intramolecular, intermolecular, or may require to be specified on a larger scale, relating to fibril structure. The horizontal element models the intrinsic resistance of the bond to bending in the case of a single molecule, or to the interaction of the molecule (or fibril) with the surrounding matrix in the more general case.

Finally, we wish to note that in indicating possible analogies between our models and rigid-rod polymer fibres we have not attempted to take into account the residual stresses which form during spinning. It has been proposed that these residual stresses have an important influence on the strain hardening behaviour of poly-*p*-phenylene benzobisthiazole fibres when tested in tension [5]. It is worth emphasizing here that the tensile stress–strain behaviour under examination in the current paper relates to fibres previously tested in compression, and it seems likely that fibres which are buckled will have a residual stress distribution quite different from that of those in the as-spun state.

5. Conclusion

A simple model has been developed to imitate the behaviour of polyaramid fibres under uniaxial compression and subsequent tension. Qualitatively, the model incorporates the observation that kinks are found to be present in Kevlar and other rigid-rod fibres which have been subjected to compressive loading and that these kinks can be removed by subsequent tensile loading. This is accompanied by a steepening of the tensile stress–strain curve and this stiffening is retained if the

fibres are unloaded then reloaded [3]. The quantitative agreement with experimental data is reasonably good with the fitting parameter, E_2 (the stiffness of the horizontal element), reasonably close to the transverse modulus, and the instability condition predicted from the parameters obtained from tensile testing is in reasonable accord with observation. Given the difficulties surrounding the testing of fibres and the consequent variablity of experimental data, the model seems to give a good description of the true material behaviour. Thus, the proposal [2] seems to be a good one that the progressive reduction and removal of kinks accounts for the shape of the tension stress–strain curve obtained with fibres which had been compressed previously along the fibre axis. This study again emphasizes the need to improve the transverse stiffness of high-performance fibres.

Acknowledgements

We are grateful to S. J. DeTeresa for valuable discussions and access to his mechanical-property data, and to R. J. Farris and E. L. Thomas for their comments and encouragement at various stages of this work. Financial support from the US Air Force through contracts F33615-78-C-5175 and F33615-82-K-5068 is gratefully acknowledged.

References

1. J. R. WHITE, *Rheol. Acta.* **20** (1981) 23.
2. S. J. DeTERESA, R. J. FARRIS and R. S. PORTER, *Polymer Composites* **3** (1982) 57.
3. S. J. DeTERESA, S. R. ALLEN, R. J. FARRIS and R. S. PORTER, *J. Mater. Sci.* **19** (1984) 57.
4. S. L. PHOENIX and J. SKELTON, *Text. Res. J.* **44** (1974) 934.
5. S. R. ALLEN, A. G. FILIPPOV, R. J. FARRIS and E. L. THOMAS, *J. Appl. Polym. Sci.* **26** (1981) 291.

Received 8 October
and accepted 26 October 1983